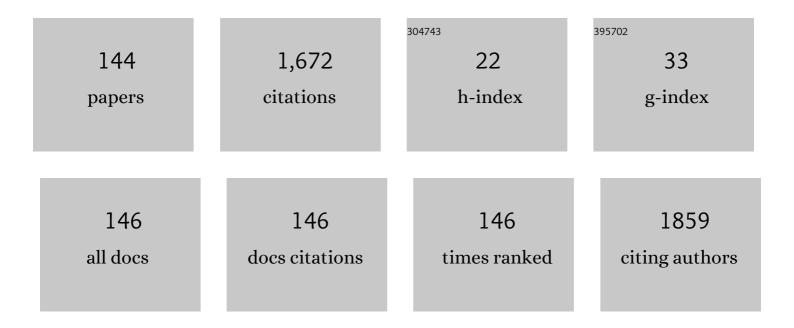
List of Publications by Year in descending order

Source: https://exaly.com/author-pdf/5186979/publications.pdf Version: 2024-02-01



IFA-CIIN DADK

#	Article	IF	CITATIONS
1	Perpendicular-spin-transfer-torque magnetic-tunnel-junction neuron for spiking neural networks depending on the nanoscale grain size of the MgO tunnelling barrier. Materials Advances, 2022, 3, 1587-1593.	5.4	0
2	Bi‣table Resistance Generation Mechanism for Oxygenated Amorphous Carbonâ€Based Resistive Randomâ€Access Memory. Advanced Electronic Materials, 2022, 8, .	5.1	4
3	Realâ€Time Correlation Detection via Online Learning of a Spiking Neural Network with a Conductiveâ€Bridge Neuron. Advanced Electronic Materials, 2022, 8, .	5.1	5
4	Surface Transformation of Spin-on-Carbon Film via Forming Carbon Iron Complex for Remarkably Enhanced Polishing Rate. Nanomaterials, 2022, 12, 969.	4.1	1
5	Polymer link breakage of polyimide-film-surface using hydrolysis reaction accelerator for enhancing chemical–mechanical-planarization polishing-rate. Scientific Reports, 2022, 12, 3366.	3.3	2
6	Impact of wet ceria abrasive size on initial step height removal efficiency for Isolated SiO2 film chemical mechanical planarization. Journal of the Korean Physical Society, 2021, 78, 51-57.	0.7	2
7	Doping-less tunnel field-effect transistors by compact Si drain frame/Si0.6Ge0.4-channel/Ge source. AIP Advances, 2021, 11, 045007.	1.3	4
8	Extremely high photoconductivity ultraviolet-light sensor using amorphous In–Ga–Zn–O thin-film-transistor. Journal of the Korean Physical Society, 2021, 78, 1221-1226.	0.7	3
9	Dishing-free chemical mechanical planarization for copper films. Colloids and Surfaces A: Physicochemical and Engineering Aspects, 2021, 616, 126143.	4.7	11
10	Enhanced performance of polymer solar cells using selective silver nanocrystal morphology. Journal of the Korean Physical Society, 2021, 79, 49.	0.7	1
11	Self-stopping slurry for planarizing extremely high surface film topography in nanoscale semiconductor devices. Journal of the Korean Physical Society, 2021, 79, 44-48.	0.7	2
12	Super fine cerium hydroxide abrasives for SiO2 film chemical mechanical planarization performing scratch free. Scientific Reports, 2021, 11, 17736.	3.3	4
13	Design of n <sup>+</sup> -base width of two-terminal-electrode vertical thyristor for cross-point memory cell without selector. Nanotechnology, 2021, 32, 14LT01.	2.6	2
14	Etch characteristics of magnetic tunnel junction materials using H <sub>2</sub> /NH <sub>3</sub> reactive ion beam. Nanotechnology, 2021, 32, 055301.	2.6	4
15	Bidirectional Electric-Induced Conductance Based on GeTe/Sb2Te3 Interfacial Phase Change Memory for Neuro-Inspired Computing. Electronics (Switzerland), 2021, 10, 2692.	3.1	2
16	Fenton Reaction for Enhancing Polishing Rate and Protonated Amine Functional Group Polymer for Inhibiting Corrosion in Ge1Sb4Te5 Film Surface Chemical-Mechanical-Planarization. Applied Sciences (Switzerland), 2021, 11, 10872.	2.5	2
17	Two-step hydrogen-ion implantation annihilation of threading dislocation defects in strain-relaxed Si0.7Ge0.3. Journal of the Korean Physical Society, 2021, 79, 1151-1156.	0.7	0
18	Scavenger with Protonated Phosphite Ions for Incredible Nanoscale ZrO2-Abrasive Dispersant Stability Enhancement and Related Tungsten-Film Surface Chemical–Mechanical Planarization. Nanomaterials, 2021, 11, 3296.	4.1	2

#	Article	IF	CITATIONS
19	Dislocation sink annihilating threading dislocations in strain-relaxed Si <sub>1â^'<i>x</i></sub> Ge <i><sub>x</sub></i> layer. Nanotechnology, 2020, 31, 12LT01.	2.6	2
20	Multi-level resistance uniformity of double pinned perpendicular magnetic-tunnel-junction spin-valve depending on top MgO barrier thickness. AIP Advances, 2020, 10, .	1.3	1
21	An electroforming-free mechanism for Cu <sub>2</sub> O solid-electrolyte-based conductive-bridge random access memory (CBRAM). Journal of Materials Chemistry C, 2020, 8, 8125-8134.	5.5	5
22	Highly Selective Polishing Rate Between a Tungsten Film and a Silicon-Dioxide Film by Using a Malic-Acid Selectivity Agent in Tungsten-Film Chemical-Mechanical Planarization. Journal of the Korean Physical Society, 2020, 76, 1127-1132.	0.7	9
23	Relationship of Free Surface Area with Oxygen Concentration in Silicon Ingot Grown by Czochralski Method for High Efficiency Solar Cells. Journal of the Korean Physical Society, 2020, 77, 940-944.	0.7	Ο
24	Interfacial Chemical and Mechanical Reactions between Tungsten-Film and Nano-Scale Colloidal Zirconia Abrasives for Chemical-Mechanical-Planarization. ECS Journal of Solid State Science and Technology, 2020, 9, 054001.	1.8	12
25	A bow-free freestanding GaN wafer. RSC Advances, 2020, 10, 21860-21866.	3.6	1
26	Influence of Scavenger on Abrasive Stability Enhancement and Chemical and Mechanical Properties for Tungsten-Film Chemical- Mechanical-Planarization. ECS Journal of Solid State Science and Technology, 2020, 9, 065001.	1.8	8
27	Double Pinned Perpendicular-Magnetic-Tunnel-Junction Spin-Valve Providing Multi-level Resistance States. Scientific Reports, 2019, 9, 11932.	3.3	11
28	Enhanced Thermal Stability in Magnetic Random-Access Memory Cells With Free Layer Composed of Multilayer Co/Pt Coupled to Co <sub>2</sub> Fe <sub>6</sub> B <sub>2</sub> With Interfacial Perpendicular Magnetic Anisotropy. IEEE Magnetics Letters, 2019, 10, 1-5.	1.1	3
29	Surface-Tensile-Stress Induced Polishing-Voids Suppression via H2O2 Oxidizer Effect in Cross-Point Phase-Change-Memory-Cells. ECS Journal of Solid State Science and Technology, 2019, 8, P667-P672.	1.8	3
30	Surface-tensile-stress induced polishing-voids in cross-point phase-change-memory cells: corrosion mechanism and solution. Semiconductor Science and Technology, 2019, 34, 065002.	2.0	2
31	Continuous Separation of Circulating Tumor Cells from Whole Blood Using a Slanted Weir Microfluidic Device. Cancers, 2019, 11, 200.	3.7	36
32	Double MgO-based Perpendicular Magnetic-Tunnel-Junction Spin-valve Structure with a Top Co2Fe6B2 Free Layer using a Single SyAF [Co/Pt]n Layer. Scientific Reports, 2018, 8, 2139.	3.3	15
33	Nanoscale CuO solid-electrolyte-based conductive-bridging, random-access memory cell with a TiN liner. Journal of the Korean Physical Society, 2018, 72, 116-121.	0.7	4
34	Novel quantum dot enhancement film with a super-wide color gamut for LCD displays. Journal of the Korean Physical Society, 2018, 72, 45-51.	0.7	9
35	Super Ultra-High Resolution Liquid-Crystal-Display Using Perovskite Quantum-Dot Functional Color-Filters. Scientific Reports, 2018, 8, 12881.	3.3	57
36	A two-terminal perpendicular spin-transfer torque based artificial neuron. Journal Physics D: Applied Physics, 2018, 51, 504002.	2.8	8

#	Article	IF	CITATIONS
37	Design of two-terminal-electrode vertical thyristor as cross-point memory cell without selector. Applied Physics Letters, 2018, 113, .	3.3	7
38	Oneâ€Pot Gramâ€Scale, Ecoâ€Friendly, and Costâ€Effective Synthesis of CuGaS <sub>2</sub> /ZnS Nanocrystals as Efficient UVâ€Harvesting Downâ€Converter for Photovoltaics. Advanced Energy Materials, 2018, 8, 1703418.	19.5	36
39	Enhanced efficiency and current density of solar cells via energy-down-shift having energy-tuning-effect of highly UV-light-harvesting Mn2+-doped quantum dots. Nano Energy, 2017, 33, 257-265.	16.0	33
40	Highly Enhanced TMR Ratio and Δ for Double MgO-based p-MTJ Spin-Valves with Top Co2Fe6B2 Free Layer by Nanoscale-thick Iron Diffusion-barrier. Scientific Reports, 2017, 7, 11907.	3.3	20
41	Electro-Forming and Electro-Breaking of Nanoscale Ag Filaments for Conductive-Bridging Random-Access Memory Cell using Ag-Doped Polymer-Electrolyte between Pt Electrodes. Scientific Reports, 2017, 7, 3065.	3.3	28
42	Effect of coupling ability between a synthetic antiferromagnetic layer and pinned layer on a bridging layer of Ta, Ti, and Pt in perpendicular-magnetic tunnel junctions. Nanotechnology, 2016, 27, 295705.	2.6	5
43	Tunneling-Magnetoresistance Ratio Comparison of MgO-Based Perpendicular-Magnetic-Tunneling-Junction Spin Valve Between Top and Bottom Co2Fe6B2 Free Layer Structure. Nanoscale Research Letters, 2016, 11, 433.	5.7	13
44	Dependency of Tunneling-Magnetoresistance Ratio on Nanoscale Spacer Thickness and Material for Double MgO Based Perpendicular-Magnetic-Tunneling-Junction. Scientific Reports, 2016, 6, 38125.	3.3	21
45	Effect of double MgO tunneling barrier on thermal stability and TMR ratio for perpendicular MTJ spin-valve with tungsten layers. Applied Physics Letters, 2016, 109, .	3.3	36
46	Dependency of tunneling magnetoresistance ratio on Pt seed-layer thickness for double MgO perpendicular magnetic tunneling junction spin-valves with a top Co <sub>2</sub> Fe <sub>6</sub> B <sub>2</sub> free layer <i>ex-situ</i> annealed at 400 °C. Nanotechnology, 2016, 27, 485203.	2.6	6
47	Perpendicular magnetic tunnel junction (p-MTJ) spin-valves designed with a top Co2Fe6B2 free layer and a nanoscale-thick tungsten bridging and capping layer. NPG Asia Materials, 2016, 8, e324-e324.	7.9	18
48	Highly enhanced perpendicular magnetic anisotropic features in a CoFeB/MgO free layer via WN diffusion barrier. Acta Materialia, 2016, 110, 217-225.	7.9	8
49	Effects of the radio-frequency sputtering power of an MgO tunneling barrier on the tunneling magneto-resistance ratio for Co <sub>2</sub> Fe <sub>6</sub> B <sub>2</sub> /MgO-based perpendicular-magnetic tunnel junctions. Journal of Materials Chemistry C, 2016, 4, 135-141.	5.5	12
50	Effect of a Co-evaporated Alq3:Liq cathode buffer layer on the performance of a polymer photovoltaic cell. Journal of the Korean Physical Society, 2015, 66, 1872-1878.	0.7	6
51	Effect of donor weight in a P3HT:PCBM blended layer on the characteristics of a polymer photovoltaic cell. Journal of the Korean Physical Society, 2015, 66, 1720-1725.	0.7	2
52	Co <sub>2</sub> Fe <sub>6</sub> B <sub>2</sub> /MgO-based perpendicular spin-transfer-torque magnetic-tunnel-junction spin-valve without [Co/Pt] <sub> <i>n</i> </sub> lower synthetic-antiferromagnetic layer. Nanotechnology, 2015, 26, 475705.	2.6	9
53	Influence of face-centered-cubic texturing of Co <sub>2</sub> Fe <sub>6</sub> B <sub>2</sub> pinned layer on tunneling magnetoresistance ratio decrease in Co <sub>2</sub> Fe <sub>6</sub> B <sub>2</sub> /MgO-based p-MTJ spin valves stacked with a [Co/Pd] <sub>n</sub> -SvAF layer. Nanotechnology. 2015. 26. 195702.	2.6	10
54	The dependency of tunnel magnetoresistance ratio on nanoscale thicknesses of Co <sub>2</sub> Fe <sub>6</sub> B <sub>2</sub> free and pinned layers for Co <sub>2</sub> Fe <sub>6</sub> B <sub>2</sub> /MgO-based perpendicular-magnetic-tunnel-junctions. Nanoscale, 2015, 7, 8142-8148.	5.6	26

#	Article	IF	CITATIONS
55	Dependency of tunneling magneto-resistance on Fe insertion-layer thickness in Co2Fe6B2/MgO-based magnetic tunneling junctions. Journal of Applied Physics, 2015, 117, .	2.5	7
56	Effect of NH3 plasma passivation on the electrical characteristics of a nanolaminated ALD HfAlO on InGaAs MOS capacitor. Journal of the Korean Physical Society, 2015, 66, 1885-1888.	0.7	1
57	Nanoscale CuO solid-electrolyte-based conductive-bridging-random-access-memory cell operating multi-level-cell and 1selector1resistor. Journal of Materials Chemistry C, 2015, 3, 9540-9550.	5.5	21
58	Low-cost and flexible ultra-thin silicon solar cell implemented with energy-down-shift via Cd <sub>0.5</sub> Zn <sub>0.5</sub> S/ZnS core/shell quantum dots. Journal of Materials Chemistry A, 2015, 3, 481-487.	10.3	16
59	High-stability transparent amorphous oxide TFT with a silicon-doped back-channel layer. Journal of the Korean Physical Society, 2014, 65, 1174-1178.	0.7	4
60	Dielectric function of Si1â^'xGex films grown on silicon-on-insulator substrates. Journal of Applied Physics, 2014, 115, 233707.	2.5	2
61	Dependency of anti-ferro-magnetic coupling strength on Ru spacer thickness of [Co/Pd]n-synthetic-anti-ferro-magnetic layer in perpendicular magnetic-tunnel-junctions fabricated on 12-inch TiN electrode wafer. Journal of Applied Physics, 2014, 116, .	2.5	10
62	Effect of nanohole structure on pyramid textured surface on photo-voltaic performance of silicon solar cell. Journal of Applied Physics, 2014, 116, 084511.	2.5	2
63	Flexible conductive-bridging random-access-memory cell vertically stacked with top Ag electrode, PEO, PVK, and bottom Pt electrode. Nanotechnology, 2014, 25, 435204.	2.6	19
64	The energy-down-shift effect of Cd <sub>0.5</sub> Zn <sub>0.5</sub> S–ZnS core–shell quantum dots on power-conversion-efficiency enhancement in silicon solar cells. Physical Chemistry Chemical Physics, 2014, 16, 18205.	2.8	23
65	Conductive-bridging random-access memory cell fabricated with a top Ag electrode, a polyethylene oxide layer, and a bottom Pt electrode. Journal of the Korean Physical Society, 2014, 64, 949-953.	0.7	4
66	Effect of core quantum-dot size on power-conversion-efficiency for silicon solar-cells implementing energy-down-shift using CdSe/ZnS core/shell quantum dots. Nanoscale, 2014, 6, 12524-12531.	5.6	41
67	Effects of metallic contaminant type and concentration on photovoltaic performance degradation of p-type silicon solar cells. Journal of the Korean Physical Society, 2013, 63, 47-52.	0.7	12
68	Effect of 8-hydroxy-quinolinato lithium thickness on the power conversion efficiency of polymer photovoltaic cells. Journal of the Korean Physical Society, 2013, 62, 490-495.	0.7	2
69	Effective multi-step Ge condensation process using intermittent SiO2 strip to obtain a high-Ge concentration and a thick Ge-on-insulator (GeOI) substrate for p-MOSFET. Journal of the Korean Physical Society, 2013, 62, 531-535.	0.7	3
70	Effect of iron(III) nitrate concentration on tungsten chemical-mechanical-planarization performance. Applied Surface Science, 2013, 282, 512-517.	6.1	29
71	Dependence of nickel gettering on crystalline nature in as-grown Czochralski silicon wafer. Journal of Crystal Growth, 2013, 365, 6-10.	1.5	3
72	Solar cell implemented with silicon nanowires on pyramid-texture silicon surface. Solar Energy, 2013, 91, 256-262.	6.1	33

#	Article	IF	CITATIONS
73	Capacitor-less memory cell fabricated on nano-scale strained Si on a relaxed SiGe layer-on-insulator. Semiconductor Science and Technology, 2013, 28, 045001.	2.0	4
74	Effects of Pt capping layer on perpendicular magnet anisotropy in pseudo-spin valves of Ta/CoFeB/MgO/CoFeB/Pt magnetic-tunneling junctions. Applied Physics Letters, 2013, 102, .	3.3	27
75	Oxygen ion drift-driven dual bipolar hysteresis curves in a single Pt/Ta2O5â^'x/TiOxNy framework. Applied Physics Letters, 2013, 103, 183510.	3.3	4
76	Correlation of the structural properties of a Pt seed layer with the perpendicular magnetic anisotropy features of full Heusler-based Co2FeAl/MgO/Co2Fe6B2 junctions via a 12-inch scale Si wafer process. Applied Physics Letters, 2013, 103, .	3.3	11
77	Effect of β-cyclodextrin and Citric Acid on Chemical Mechanical Polishing of Polycrystalline Ge2Sb2Te5in H2O2Containing Slurry. ECS Journal of Solid State Science and Technology, 2013, 2, P299-P304.	1.8	2
78	Nonvolatile Polymer Memory-Cell Embedded with Ni Nanocrystals Surrounded by NiO in Polystyrene. IEICE Transactions on Electronics, 2013, E96.C, 699-701.	0.6	0
79	Effect of Slurry pH and H2O2on Polycrystalline Ge2Sb2Te5CMP Performance. Journal of the Electrochemical Society, 2012, 159, C546-C551.	2.9	7
80	Polymer photovoltaic cell embedded with p-type single walled carbon nanotubes fabricated by spray process. Nanotechnology, 2012, 23, 325401.	2.6	8
81	High polishing selectivity ceria slurry for formation of top electrode in spin-transfer torque magnetic random access memory. Thin Solid Films, 2012, 522, 212-216.	1.8	1
82	Effect of Potassium Ferricyanide in the Acid Solution on Performance of Tungsten Chemical Mechanical Planarization. Journal of the Electrochemical Society, 2012, 159, H363-H366.	2.9	7
83	Effect of MeV nitrogen ion implantation on the resistivity transition in Czochralski silicon wafers. Journal of the Korean Physical Society, 2012, 61, 1981-1985.	0.7	0
84	Effect of a thermally evaporated bis (2-methyl-8-quninolinato)-4-phenylphenolate cathode buffer layer on the performance of polymer photovoltaic cells. Journal of the Korean Physical Society, 2012, 61, 507-512.	0.7	1
85	Nonvolatile Hybrid Memory Cell Embedded with Ni Nanocrystals in Poly(3-hexylthiophene). Japanese Journal of Applied Physics, 2012, 51, 120202.	1.5	1
86	Small-Molecule Nonvolatile Memory Cells Embedded with Ti Nanocrystals Surrounded by TiO\$_{2} Tunneling Barrier. Applied Physics Express, 2011, 4, 105003.	2.4	0
87	Dependence of Ag Film Thickness on Ag Nanocrystals Formation to Fabricate Polymer Nonvolatile Memory. IEICE Transactions on Electronics, 2011, E94-C, 850-853.	0.6	0
88	Dependence of nonvolatile memory characteristics on curing temperature for polymer memory-cell embedded with Au nanocrystals in poly(N-vinylcarbazole). Current Applied Physics, 2011, 11, e25-e29.	2.4	8
89	Effect of Small-Molecule Layer Thickness on Nonvolatile Memory Characteristics for Small-Molecule Memory-cells. Electrochemical and Solid-State Letters, 2011, 14, H277.	2.2	4
90	Chemical Mechanical Planarization Mechanism for Nitrogen-Doped Polycrystalline Ge <sub>2</sub> Sb <sub>2</sub> Te <sub>5</sub> Film Using Nitric Acidic Slurry Added with Hydrogen Peroxide. Journal of the Electrochemical Society, 2011, 158, H666-H670.	2.9	15

#	Article	IF	CITATIONS
91	A multi-level capacitor-less memory cell fabricated on a nano-scale strained silicon-on-insulator. Nanotechnology, 2011, 22, 315201.	2.6	3
92	Capacitor-less memory-cell fabricated on nanoscale unstrained Si layer on strained SiGe layer-on-insulator. Applied Physics Letters, 2010, 96, 163508.	3.3	4
93	Nonvolatile memory characteristics of small-molecule memory cells with electron-transport and hole-transport bilayers. Current Applied Physics, 2010, 10, e37-e41.	2.4	5
94	Effect of NiOx thin layer fabricated by oxygen-plasma treatment on polymer photovoltaic cell. Solar Energy Materials and Solar Cells, 2010, 94, 1591-1596.	6.2	50
95	Effect of interface chemical properties on nonvolatile memory characteristics for small-molecule memory cells embedded with Ni nano-crystals surrounded by NiO. Current Applied Physics, 2010, 10, e32-e36.	2.4	4
96	Increase in the Adsorption Density of Anionic Molecules on Ceria for Defect-Free STI CMP. Journal of the Electrochemical Society, 2010, 157, H72.	2.9	17
97	Multiselectivity Chemical Mechanical Polishing for NAND Flash Memories beyond 32 nm. Journal of the Electrochemical Society, 2010, 157, H607.	2.9	8
98	Micro Defect Size in Si Single Crystal Grown by Czochralski Method. Japanese Journal of Applied Physics, 2010, 49, 121301.	1.5	5
99	Effect of Hydroxyethyl Cellulose Concentration on Surface Qualities of Silicon Wafer after Touch Polishing Process. Electrochemical and Solid-State Letters, 2010, 13, H147.	2.2	15
100	Role of Hydrogen Peroxide in Alkaline Slurry on the Polishing Rate of Polycrystalline Ge[sub 2]Sb[sub 2]Te[sub 5] Film in Chemical Mechanical Polishing. Electrochemical and Solid-State Letters, 2010, 13, H155.	2.2	28
101	Potassium Permanganate as Oxidizer in Alkaline Slurry for Chemical Mechanical Planarization of Nitrogen-doped Polycrystalline Ge[sub 2]Sb[sub 2]Te[sub 5] Film. Journal of the Electrochemical Society, 2010, 157, H1036.	2.9	17
102	Optimal Channel Ion Implantation for High Memory Margin of Capacitor-Less Memory Cell Fabricated on Fully Depleted Silicon-on-Insulator. Japanese Journal of Applied Physics, 2010, 49, 036507.	1.5	1
103	Effect of Organic Additive on Surface Roughness of Polycrystalline Silicon Film after Chemical Mechanical Polishing. Japanese Journal of Applied Physics, 2010, 49, 010216.	1.5	4
104	Fabricated nonvolatile memory with Ag nano-crystals embedded in PVK. , 2010, , .		0
105	Dependence of memory margin of Cap-less memory cells on top Si thickness. Applied Physics Letters, 2009, 94, 023508.	3.3	9
106	The effect of donor layer thickness on the power conversion efficiency of organic photovoltaic devices fabricated with a double small-molecular layer. Nanotechnology, 2009, 20, 335201.	2.6	5
107	Comparative study of self-heating effect on electron mobility in nano-scale strained silicon-on-insulator and strained silicon grown on relaxed SiGe-on-insulator n-metal–oxide–semiconductor field-effect transistors. Semiconductor Science and Technology, 2009, 24. 035014.	2.0	7
108	Effect of Interface Thickness on Power Conversion Efficiency of Polymer Photovoltaic Cells. Electronic Materials Letters, 2009, 5, 47-50.	2.2	44

#	Article	IF	CITATIONS
109	Multilevel Nonvolatile Small-Molecule Memory Cell Embedded with Ni Nanocrystals Surrounded by a NiO Tunneling Barrier. Nano Letters, 2009, 9, 1713-1719.	9.1	103
110	Effect of Metal-Reflection and Surface-Roughness Properties on Power-Conversion Efficiency for Polymer Photovoltaic Cells. Journal of Physical Chemistry C, 2009, 113, 21915-21920.	3.1	43
111	Impact of donor, acceptor, and blocking layer thickness on power conversion efficiency for small-molecular organic solar cells. Synthetic Metals, 2009, 159, 1705-1709.	3.9	27
112	Crystalline structure of ceria particles controlled by the oxygen partial pressure and STI CMP performances. Ultramicroscopy, 2008, 108, 1292-1296.	1.9	20
113	Dependence of temperature and self-heating on electron mobility in ultrathin body silicon-on-insulator n-metal-oxide-semiconductor field-effect transistors. Journal of Applied Physics, 2008, 103, .	2.5	8
114	Effect of Au Nanocrystals Embedded in Conductive Polymer on Non-volatile Memory Window. Materials Research Society Symposia Proceedings, 2008, 1071, 1.	0.1	0
115	Hole Mobility Behavior in Strained SiGe-on-SOI p-MOSFETs. ECS Transactions, 2008, 13, 345-350.	0.5	2
116	Effect of abrasive material properties on polishing rate selectivity of nitrogen-doped Ge <sub>2</sub> Sb <sub>2</sub> Te <sub>5</sub> to SiO <sub>2</sub> film in chemical mechanical polishing. Journal of Materials Research, 2008, 23, 3323-3329.	2.6	12
117	Constraints on removal of Si <sub>3</sub> N <sub>4</sub> film with conformation-controlled poly(acrylic acid) in shallow-trench isolation chemical–mechanical planarization (STI CMP). Journal of Materials Research, 2008, 23, 49-54.	2.6	15
118	Silicon thickness fluctuation scattering dependence of electron mobility in ultrathin body silicon-on-insulator n-metal-oxide-semiconductor field-effect transistors. Journal of Applied Physics, 2008, 103, 084503.	2.5	5
119	Selectivity Enhancement in the Removal of SiO2 and Si3N4 Films with Addition of Triethanolamine in a Ceria Slurry during Shallow Trench Isolation Chemical Mechanical Polishing. Journal of the Korean Physical Society, 2008, 53, 1337-1342.	0.7	4
120	Hole Mobility Enhancement in Strained SiGe Grown on Silicon-on-Insulator p-MOSFETs. Journal of the Korean Physical Society, 2008, 53, 2171-2174.	0.7	4
121	Dependence of Electrical Characteristics on Si Thickness and Ge Concentration for Unstrained Si Grown on Strained SiGe-on-Insulator n-Metal–Oxide–Semiconductor Field-Effect Transistor. Japanese Journal of Applied Physics, 2007, 46, 3324-3329.	1.5	7
122	Impact of the top silicon thickness on phonon-limited electron mobility in (110)-oriented ultrathin-body silicon-on-insulator n-metal-oxide-semiconductor field-effect transistors. Journal of Applied Physics, 2007, 102, 063520.	2.5	9
123	Effects of abrasive particle size and molecular weight of poly(acrylic acid) in ceria slurry on removal selectivity of SiO2/Si3N4 films in shallow trench isolation chemical mechanical planarization. Journal of Materials Research, 2007, 22, 777-787.	2.6	16
124	Effect of O2 Plasma Treatment on Hole-Injection Enhancement for Organic Light-Emitting Devices with Transparent Au:Al Anodes. Journal of the Korean Physical Society, 2007, 50, 1327.	0.7	5
125	Extremely proximity gettering for semiconductor devices. Materials Science and Engineering B: Solid-State Materials for Advanced Technology, 2006, 134, 249-256.	3.5	9
126	Strained Si engineering for nanoscale MOSFETs. Materials Science and Engineering B: Solid-State Materials for Advanced Technology, 2006, 134, 142-153.	3.5	7

#	Article	IF	CITATIONS
127	Effect of Calcination Process on Synthesis of Ceria Particles, and Its Influence on Shallow Trench Isolation Chemical Mechanical Planarization Performance. Japanese Journal of Applied Physics, 2006, 45, 4893-4897.	1.5	7
128	Atomic force microscopy study of the role of molecular weight of poly(acrylic acid) in chemical mechanical planarization for shallow trench isolation. Journal of Materials Research, 2006, 21, 473-479.	2.6	20
129	Effects of Abrasive Size and Surfactant Concentration on the Non-Prestonian Behavior of Ceria Slurry in Shallow Trench Isolation Chemical Mechanical Polishing. Japanese Journal of Applied Physics, 2005, 44, L136-L139.	1.5	9
130	Dependence of pH, Molecular Weight, and Concentration of Surfactant in Ceria Slurry on Saturated Nitride Removal Rate in Shallow Trench Isolation Chemical Mechanical Polishing. Japanese Journal of Applied Physics, 2005, 44, 4752-4758.	1.5	11
131	Influence of Physical Characteristics of Ceria Particles on Polishing Rate of Chemical Mechanical Planarization for Shallow Trench Isolation. Japanese Journal of Applied Physics, 2004, 43, 7427-7433.	1.5	23
132	Dependence of Nanotopography Impact on Abrasive Size and Surfactant Concentration in Ceria Slurry for Shallow Trench Isolation Chemical Mechanical Polishing. Japanese Journal of Applied Physics, 2004, 43, L1-L4.	1.5	13
133	Extended Defects and Pile-Up of Interstitial Oxygen in Silicon Wafer Due to MeV-Level Nitrogen Ion Implantation. Japanese Journal of Applied Physics, 2004, 43, 6854-6857.	1.5	5
134	Effect of Molecular Weight of Surfactant in Nano Ceria Slurry on Shallow Trench Isolation Chemical Mechanical Polishing (CMP). Japanese Journal of Applied Physics, 2004, 43, L1060-L1063.	1.5	23
135	Effects of Grain Size and Abrasive Size of Polycrystalline Nano-particle Ceria Slurry on Shallow Trench Isolation Chemical Mechanical Polishing. Japanese Journal of Applied Physics, 2004, 43, L365-L368.	1.5	16
136	Dependence of crystal nature on the gettering efficiency of iron and nickel in a Czochralski silicon wafer. Microelectronic Engineering, 2003, 66, 247-257.	2.4	8
137	Influence of the electrokinetic behaviors of abrasive ceria particles and the deposited plasma-enhanced tetraethylorthosilicate and chemically vapor deposited Si <sub>3</sub> N <sub>4</sub> films in an aqueous medium on chemical mechanical planarization for shallow trench isolation. Journal of Materials Research, 2003, 18, 2163-2169.	2.6	37
138	Surfactant Effect on Oxide-to-Nitride Removal Selectivity of Nano-abrasive Ceria Slurry for Chemical Mechanical Polishing. Japanese Journal of Applied Physics, 2003, 42, 5420-5425.	1.5	32
139	Effects of Abrasive Morphology and Surfactant Concentration on Polishing Rate of Ceria Slurry. Japanese Journal of Applied Physics, 2003, 42, 1150-1153.	1.5	42
140	Effects of the Physical Characteristics of Cerium Oxide on Plasma-Enhanced Tetraethylorthosiliate Removal Rate of Chemical Mechanical Polishing for Shallow Trench Isolation. Japanese Journal of Applied Physics, 2003, 42, 1227-1230.	1.5	20
141	Spectral Analyses on Pad Dependency of Nanotopography Impact on Oxide Chemical Mechanical Polishing. Japanese Journal of Applied Physics, 2002, 41, L17-L19.	1.5	11
142	Sputterâ€grown GeTe/Sb 2 Te 3 superlattice interfacial phase change memory for low power and multiâ€levelâ€cell operation. Electronics Letters, 0, , .	1.0	3
143	Two-terminal vertical thyristor using Schottky contact emitter to improve thermal instability. Nano Futures, 0, , .	2.2	1
144	Layerâ€dependent effects of interfacial phase change memory for an artificial synapse. Physica Status Solidi - Rapid Research Letters, 0, , .	2.4	2